


## Neutron scattering study on dimerized $4f^1$ intermetallic compound $Ce_5Si_3$

Daichi Ueta <sup>1,\*</sup>, Yuki Iwata,<sup>2</sup> Riki Kobayashi <sup>2</sup>, Keitaro Kuwahara,<sup>3</sup> Takatsugu Masuda <sup>1,4</sup> and Shinichi Itoh <sup>1</sup>

<sup>1</sup>*Institute of Materials Structure Science, High Energy Accelerator Research Organization, 1-1 Oho, Tsukuba 305-0801, Japan*

<sup>2</sup>*Faculty of Science, University of the Ryukyus, 1 Senbaru, Nishihara-cho 903-0123, Japan*

<sup>3</sup>*Graduate School of Science and Engineering, Ibaraki University, 2-1-1 Mito, Ibaraki 310-8512, Japan*

<sup>4</sup>*Neutron Science Laboratory, Institute for Solid State Physics, The University of Tokyo, 5-1-5 Kashiwanoha, Kashiwa 277-8581, Japan*



(Received 21 July 2023; revised 2 March 2024; accepted 22 April 2024; published 9 May 2024)

$Ce_5Si_3$  exhibits geometrical frustration in its crystal structure and possesses a Schottky-type anomaly, implying dimer formation based on specific heat measurements. We performed inelastic neutron scattering experiments on polycrystalline samples to observe microscopical evidence of dimer formation. Crystalline electric field excitations were observed at 17, 27, 39, and 63 meV, and magnetic excitation caused by spin-dimer formation with dispersion was observed at approximately 0.6 meV. The magnetic excitation observed at low energies may originate from spin-dimer formation, which exhibits large dispersion that cannot be explained using the conventional Shastry–Sutherland lattice model, implying that the excited-state pseudotriplet may split.

DOI: [10.1103/PhysRevB.109.205127](https://doi.org/10.1103/PhysRevB.109.205127)

### I. INTRODUCTION

Geometrical frustration in crystal structures can help derive typical physical properties and has been an interesting in condensed matter researchers. Recently, quantum spin liquids (QSLs) and magnetic skyrmions have attracted attention in such systems. In  $f$ -electron systems, typical properties originating from geometrical frustration, such as spin dimer [1,2], partial order [3,4], and spin liquid/ice [5–11], have been reported. One of the main features of  $f$ -electron systems is the interaction between  $f$  electrons via conduction electrons. A relatively large value of the electronic specific heat coefficient has been reported for many cerium compounds, such as  $Ce_5Si_3$  [12], suggesting that the  $f$  electrons contribute to the conduction. Therefore, the combination of nonlocalized  $4f$  electrons and frustration may help explore the new phenomena of physical properties.

Frustration in square lattices was considered by Shastry and Sutherland [13]. They realized a frustrated system in a square lattice (Shastry–Sutherland lattice: SSL) by treating the intersquare lattice interaction as nearest-neighbor  $J$  and the intrasquare lattice interaction as next-nearest-neighbor  $J'$ . Using the two-dimensional quantum Heisenberg model, it has been calculated theoretically that the spin-dimer state is stable for  $\alpha = J'/J < 0.677$  and the plaquette-singlet state is stable for  $0.677 < \alpha < 0.86(0.77)$  [14,15]. More recently, it has been reported that a QSL appears between the plaquette-singlet phase and the antiferromagnetic phase near  $\alpha = 0.86(0.77)$  in a SSL model [16]. In a three-dimensional system stacked with SSL layers, it is suggested that in-plane dimers can be formed roughly under the  $0.75J - J' - J'' > 0$  condition [17], where  $J''$  denotes the interaction between the SSL layers.

$SrCu_2(BO_3)_2$  is the only compound for which SSL has been realized with  $S = 1/2$  and has been studied by a variety of methods [18]. A Schottky-type anomaly suggesting spin-dimer formation was observed at  $T = 7.5$  K in the specific heat measurement [19], and dimer excitation with small dispersion below 0.2 meV was observed in a neutron experiment [20]. In addition, excitations suggesting a plaquette-singlet state due to pressure effects have been observed in neutron experiments [21]. More recent nuclear magnetic resonance studies have observed gapless behavior between the plaquette-singlet phase and the antiferromagnetic phase that could be connected to a QSL [22].

$Ce_5Si_3$  is another candidate for an SSL model. Figure 1(a) shows the crystal structure of tetragonal  $Ce_5Si_3$  with a  $Cr_5B_3$ -type structure [23]. In this structure, cerium atoms responsible for magnetism occupy two sites shown as blue and brown balls, with an existence ratio of  $Ce(1):Ce(2) = 1:4$ . In particular, the  $Ce(2)$  site, shown as brown balls, forms an SSL. Figure 1(b) shows an extract of the adjacent  $Ce(2)$  sites and viewed from the  $c$  axis. The darker colors depict the upper layers, and the lighter colors depict the lower layers. In the SSL model, spin dimers can form between the nearest-neighbor atoms shown by the green broken line at the  $Ce(2)$  site in Fig. 1(b). Although the SSL model represents a frustrated lattice in a two-dimensional plane,  $Ce_5Si_3$  exhibits a bilayer system of the SSL layers with  $Ce(2)$ , and a  $Ce(2)$  layer may interact with the neighboring  $Ce(1)$  layer. In other words,  $Ce_5Si_3$  is considered to form dimers, even though the interactions are three dimensional. However, dimer formation in  $4f$ -electron systems has been reported for isolated dimers of  $YbAl_3C_3$  [1,2], and the origin of dimer formation in  $4f$ -electron systems with very weak direct interactions is yet to be explored.

$Ce_5Si_3$  is suggested to form spin dimers at the  $Ce(2)$  site [12]. From the specific heat measurements,  $\lambda$ -type ( $T_N = 12$  K) and Schottky-type ( $T_d = 2.5$  K) anomalies were observed, and the magnetic entropy at 20 K is reported to

\*dueta@post.kek.jp

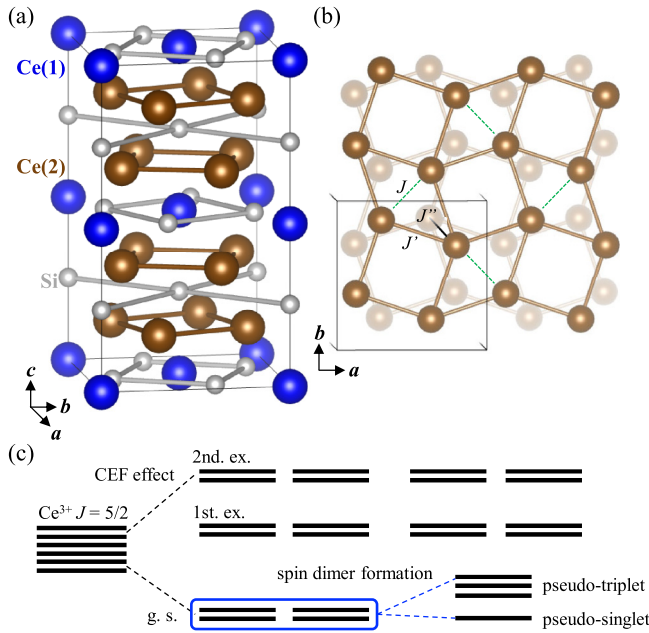


FIG. 1. (a) Crystal structure of  $\text{Ce}_5\text{Si}_3$  illustrated using VESTA [23]. Blue and brown balls exhibit the cerium atoms, and silver balls exhibit the silicon atoms. (b) SSL cerium layers at the  $ab$  plane. The green broken line connects the nearest-neighbor atoms in the SSL. (c) CEF splitting in  $\text{Ce}^{3+}$  ions and splitting of the ground-state doublet due to spin-dimer formation at the Ce(2) site.

reach  $4.5R\ln 2/\text{mol}$  [12,24]. The magnetic entropy exceeds  $2R\ln 2/\text{mol}$  between  $T_d$  and  $T_N$ . These results indicate that the anomaly observed in  $T_d$  originate from the magnetic moment of the Ce(2) site with four cerium atoms in the unit cell. Other than magnetic susceptibility and electrical resistivity, no anomalies due to magnetic transition at zero magnetic field have been observed [12,24,25]. In addition, a decrease in the magnetic susceptibility with  $H // [100]$  was not observed below  $T_N$  [24–26]. These results suggest that the magnetic moment of the Ce(2) site is not magnetically ordered. Therefore, the magnetic moments at the Ce(2) site can form spin dimers in the SSL model, splitting the ground-state doublet into a ground-state pseudosinglet and excited-state pseudotriplet [Fig. 1(c)], which leads to the Schottky-type anomaly observed in the specific heat measurements. By contrast, the anomaly at  $T_N$  suggests a magnetic transition, with a released entropy of approximately  $R\ln 2/\text{mol}$ . The magnetic susceptibility with  $H // [001]$  decreases below  $T_N$  [24–26], suggesting that the magnetic moments of the Ce(1) site exhibit antiferromagnetic ordering along the  $c$  axis.

In neutron experiments, dispersionless magnetic excitation with a gap of  $\Delta_d \sim 8$  K ( $\Delta_d = 3.2T_d$ ) can be observed, such as excitations in the well-known SSL system, i.e.,  $\text{SrCu}_2(\text{BO}_3)_2$  [13,20]. Therefore, in this work we attempted to observe magnetic excitations by performing inelastic neutron scattering (INS) experiments to determine the crystalline electric field (CEF) level schemes and to obtain microscopic evidence of the formation of spin dimers at the Ce(2) sites of  $\text{Ce}_5\text{Si}_3$ . In this paper, after describing the details of the experimental procedures, we report the CEF level schemes and low-energy excitation obtained in the INS experiments

and discuss low-energy magnetic excitation due to spin-dimer formation.

## II. EXPERIMENTAL PROCEDURE

Single-crystal samples of  $\text{Ce}_5\text{Si}_3$  and  $\text{La}_5\text{Si}_3$  were grown using a self-flux method [26]. Constituent elements Ce/La (3N), whose oxide film had been removed, and Si (5N) were placed in a silica tube along with an appropriate amount of cerium as a flux. Subsequently, the sealed silica ampoule was heated in a box furnace up to  $1100^\circ\text{C}$  and then slowly cooled to  $750^\circ\text{C}$ . After cooling, the excess flux was removed using a centrifuge, and the flux that remained on the surface of the samples was removed by oxidation in air. As Ce-rich compounds can ignite when ground in air, the obtained samples were evaluated using a single-crystal x-ray diffractometer and were found to be single-crystal samples of  $\text{Ce}_5\text{Si}_3$ .

INS experiments were performed using the High Resolution Chopper spectrometer (HRC) installed at BL12 in J-PARC MLF [27]. After wrapping approximately 10 g of a single-crystal sample with a typical size of  $5 \times 5 \times 2 \text{ mm}^3$  with 10 mg in aluminum foil, it was enclosed in an aluminum cell with helium exchange gas and cooled to 0.3 K using a one-shot-type  $^3\text{He}$  refrigerator. Single-crystal samples were treated as a polycrystalline sample by using them without orientation, because polycrystalline samples prepared by arc melting can form a separate phase via incongruent melting and, as mentioned above, there is a risk of ignition owing to the grinding of the single-crystal samples. To observe CEF excitations and spin-dimer excitation, the incident neutron energy was set to  $E_i = 153.5$  and 3 meV. Nonmagnetic and isostructural  $\text{La}_5\text{Si}_3$  was used to estimate the phonon contribution to scattering. The acquired data were normalized based on the number of protons injected into the neutron production target, which is proportional to the measuring time, and the contribution of the aluminum cell was subtracted. The data were normalized with consistent nonmagnetic backgrounds, and the magnetic component was extracted.

Specific heat and magnetization measurements were performed using a physical property measurement system (PPMS; Quantum Design, Inc.) and magnetic property measurement system (MPMS; Quantum Design, Inc.), respectively. The specific heat measurement using the thermal relaxation method was performed with a  $^3\text{He}$  cooling option at 0.5–15 K. For magnetization measurements, the sample installed in the MPMS was cooled to 1.8 K under zero magnetic field, and magnetization was measured up to 300 K when the temperature was increased by applying 1 kOe of magnetic field.

## III. RESULTS AND DISCUSSION

### A. Crystalline electric field excitations

Before observing the magnetic excitation caused by dimer formation, it is necessary to determine other magnetic excitations. In tetragonal and lower symmetry,  $\text{Ce}^{3+}$  ion splits into three doublets owing to the CEF effect. In other words, four CEF excitations are expected to be observed in  $\text{Ce}_5\text{Si}_3$ , where two sites are occupied by cerium atoms. To determine the CEF level scheme, the INS experiments were performed at

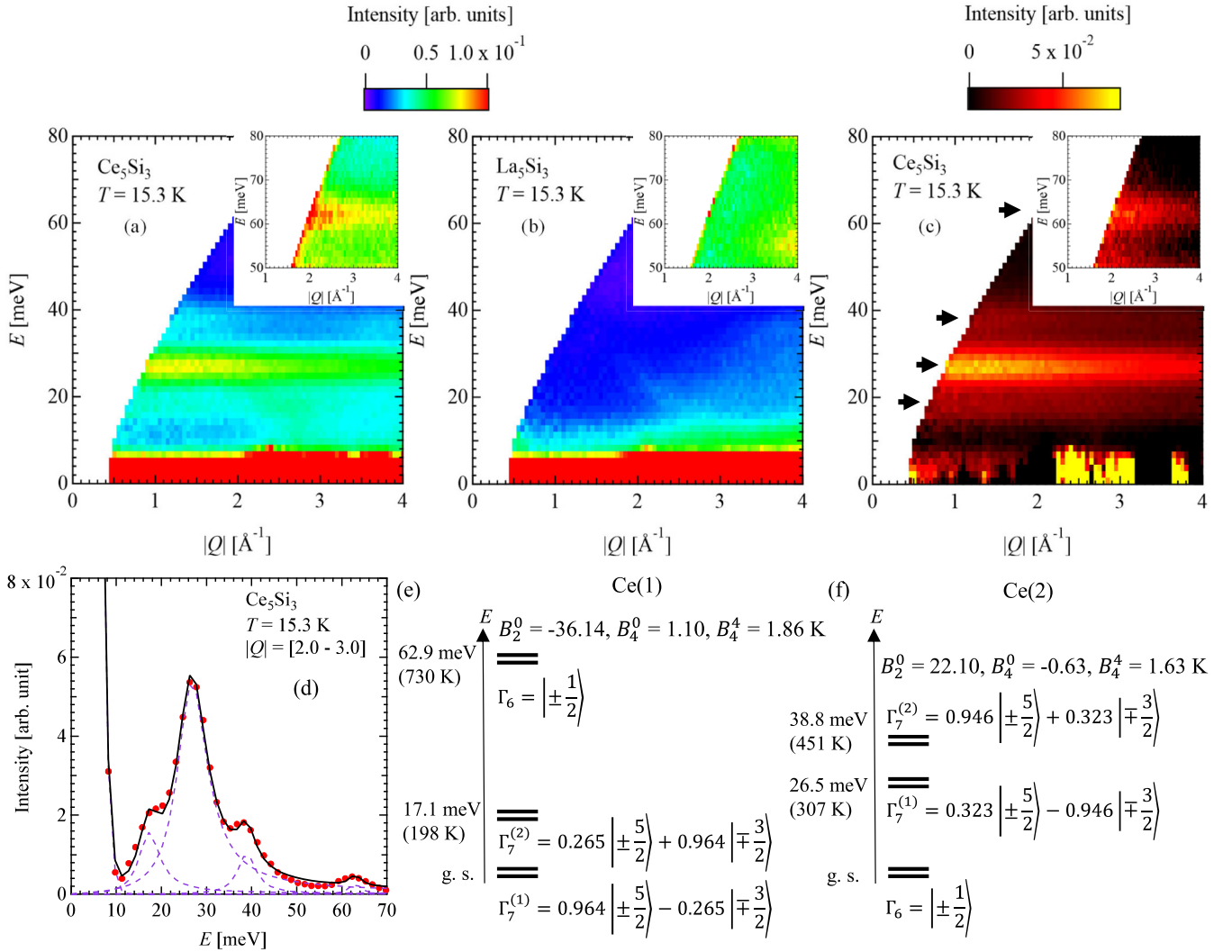


FIG. 2. Color-coded plots of INS intensities measured on the HRC with  $E_i = 153$  meV for (a)  $\text{Ce}_5\text{Si}_3$ , (b)  $\text{La}_5\text{Si}_3$ , and (c) magnetic scattering of  $\text{Ce}_5\text{Si}_3$  at 15.3 K. The insets show the data above 50 meV with the color scale changed to clarify the excitation. (d) A section of magnetic scattering integrated over  $|Q|$  from 2.0 to 3.0  $\text{\AA}^{-1}$ . The black solid line shows the fitting results, and the dashed lines represent the fitting components of the elastic scattering and CEF excitations, respectively. The vertical bars represent the statistical errors. The CEF level scheme of  $\text{Ce}_5\text{Si}_3$  at (e) Ce(1) and (f) Ce(2) sites evaluated based on the analysis of the INS data.

15.3 K, which is higher than the magnetic transition temperature ( $T_N \simeq 12$  K [24]), with the incident neutron energy of  $E_i = 153.5$  meV and a Fermi chopper frequency of 500 Hz.

Figures 2(a) and 2(b) show the color-coded plots of INS intensities of  $\text{Ce}_5\text{Si}_3$  and nonmagnetic isostructural  $\text{La}_5\text{Si}_3$ . The vertical axis represents the energy transfer  $E$ , and the horizontal axis represents the scattering vector  $|Q|$ . The insets show the plots for  $50 \leq E \leq 80$  meV, with the color scale changed to clarify the excitation. Figure 2(c) shows the results of subtracting the  $\text{La}_5\text{Si}_3$  data from the  $\text{Ce}_5\text{Si}_3$  data to clarify the magnetic scattering contribution. Strong magnetic scattering intensities are evident at approximately 17, 27, 39, and 63 meV (black arrows). The one-dimensional cutout of  $2 \leq |Q| \leq 3 \text{\AA}^{-1}$  is depicted by the red circles in Fig. 2(d), which also indicates four peaks in the figure. Figure 3(a) shows the  $Q$  dependence of the observed magnetic scattering, and these behaviors are well explained by the magnetic form factor of the  $\text{Ce}^{3+}$  ions. Therefore, we focused on these four

peaks and performed CEF model calculations to determine the CEF level scheme of  $\text{Ce}_5\text{Si}_3$ .

The CEF Hamiltonian for  $\text{Ce}^{3+}$  ions with  $J = 5/2$  tetragonal point symmetry is described as follows:

$$\mathcal{H}_{\text{CEF}} = B_2^0 O_2^0 + B_4^0 O_4^0 + B_4^4 O_4^4, \quad (1)$$

TABLE I. Temperature dependence of the CEF parameters and CEF levels on  $\text{Ce}_5\text{Si}_3$ .  $B_l^m$  represent the CEF parameters [28], and  $\Delta_1$  and  $\Delta_2$  represent the energy difference from the ground state to the first and second excited states, respectively.

	Temperature [K]	$B_2^0$ [K]	$B_4^0$ [K]	$B_4^4$ [K]	$\Delta_1$ [meV]	$\Delta_2$ [meV]
Ce(1)	15.3	-36.14	1.10	1.86	17.1	62.9
	1.0	-35.51	1.06	2.88	19.9	63.1
Ce(2)	15.3	22.10	-0.63	1.63	26.5	38.8
	1.0	22.16	-0.67	1.95	27.0	39.7

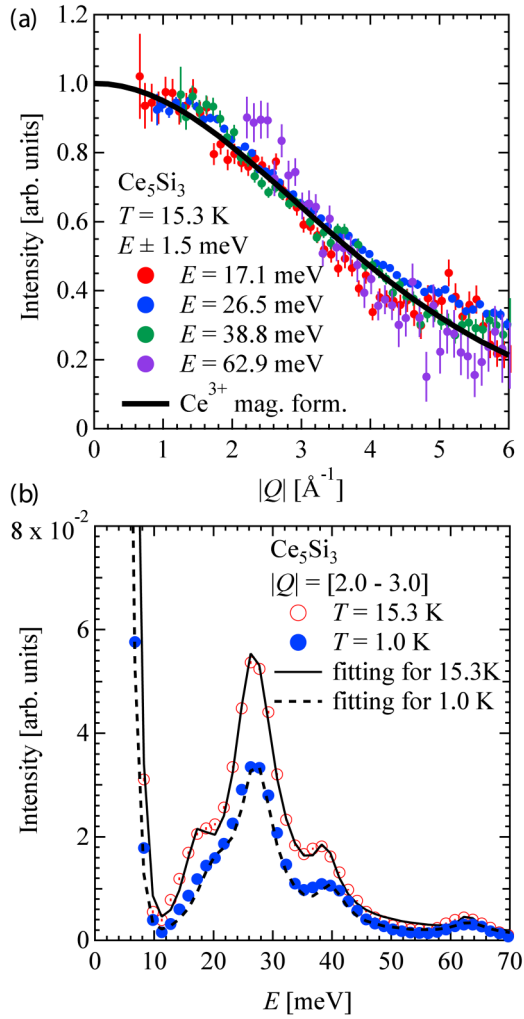


FIG. 3. (a)  $|Q|$  dependence of magnetic scatterings observed at around  $E = 17.1$  (red), 26.5 (blue), 38.8 (green), and 62.9 (purple) meV and behavior of magnetic form factor of  $\text{Ce}^{3+}$  ions. (b) Energy dependence of magnetic scattering intensity of  $\text{Ce}_5\text{Si}_3$  at 15.3 K (red circles) and 1.0 K (blue circles). The black solid line and the black broken lines show the fitting results at 15.3 K and 1.0 K, respectively. The CEF parameters and levels obtained from this fitting are listed in Table I. The vertical bars in (a) and (b) represent the statistical errors.

where  $B_l^m$  denotes the CEF parameters and  $O_l^m$  denotes Stevens' equivalent operators [28]. The sixth-order parameters in the CEF Hamiltonian are zero-valued for  $\text{Ce}^{3+}$  ions and therefore omitted in the calculation. The point symmetry of the Ce(2) site is lower than that of the tetragonal symmetry, and the  $B_2^2$  and  $B_4^2$  terms are added to the CEF Hamiltonian. Although  $B_2^2$  is responsible for hybridization  $\Gamma_6$  and  $\Gamma_7$ , the contribution of this term reported in previous studies is small [25], and the observed neutron intensities discussed below can be explained without this term. The  $B_4^2$  term is responsible for in-plane anisotropy; however, no in-plane anisotropy has been reported in  $\text{Ce}_5\text{Si}_3$  [25]. Therefore, the tetragonal CEF Hamiltonian described above is used for this analysis. By diagonalizing this Hamiltonian, three doublets with different energies and corresponding wave functions can be obtained.

In the INS experiment, the transition from one level to another was observed as neutron energy transfer and the transition probability was considered as the scattering intensity, represented by the dynamical susceptibility  $\chi''$ :

$$\chi''(E) \propto \frac{E}{Z} \sum_{i,f}^{\varepsilon_i \neq \varepsilon_f} \sum_{\perp=x,y,z} |\langle f | J_{\perp} | i \rangle|^2 F(E)$$

$$Z = \sum \exp(\Delta_l/k_B T)$$

$$F(E) = \frac{\exp(-\frac{\varepsilon_i}{k_B T}) - \exp(-\frac{\varepsilon_f}{k_B T})}{\varepsilon_f - \varepsilon_i}$$

$$\times \frac{\Gamma_{\text{CEF}}(i, f)}{\{E - (\varepsilon_f - \varepsilon_i)\}^2 + \Gamma_{\text{CEF}}^2(i, f)}, \quad (2)$$

where  $Z$  is the partition function and  $\Delta$  is the energy difference from the ground state of the corresponding wave function  $l$  ( $l = 1, 2, \dots, 6$ ).  $\varepsilon_i$  and  $\varepsilon_f$  are the respective energy eigenvalues of the initial and final states,  $|i\rangle$  and  $|f\rangle$ ,  $J_{\perp}$  ( $\perp = x, y, z$ ) is the magnetization component perpendicular to the scattering vector  $Q$ , and  $\Gamma$  is the width of the function. In  $\text{Ce}_5\text{Si}_3$  there are two cerium sites; thus, fitting was performed with a function using the existence ratios.

$$I(E) = G(E) + A_{\text{CEF}} \chi''_{\text{Ce}(1)}(E) + 4A_{\text{CEF}} \chi''_{\text{Ce}(2)}(E)$$

$$G(E) = A_G \exp \left\{ -\ln 2 \left( \frac{E}{\Gamma_G/2} \right)^2 \right\}, \quad (3)$$

where  $A$  is a scale factor of the function corresponding to the respective subscripts and  $G(E)$  is a Gaussian function representing elastic scattering.

The black solid line in Fig. 2(d) shows the fitting results. The fitting results indicate the presence of CEF excitations of  $\text{Ce}_5\text{Si}_3$  centered at 17.1 and 62.9 meV on the Ce(1) site with CEF parameters of  $B_2^0 = -36.14(55)$  K,  $B_4^0 = 1.10(3)$  K, and  $B_4^4 = 1.86(36)$  K, and at 26.5 and 38.8 meV on Ce(2) site with CEF parameters of  $B_2^0 = 22.10(32)$  K,  $B_4^0 = -0.63(1)$  K, and  $B_4^4 = 1.63(12)$  K. We considered other combinations of peaks; however, there was only one solution that could address the existence ratio of 1:4 and the behavior of the magnetic susceptibility described below. The resulting CEF level schemes of cerium sites in  $\text{Ce}_5\text{Si}_3$  are shown in Figs. 2(e) and 2(f).

Figure 3(b) shows the temperature evolution of the magnetic scattering intensity for a one-dimensional cutout of  $2 \leq |Q| \leq 3 \text{\AA}^{-1}$ . Although the ground state may split at 15.3 K due to spin-dimer formation, it was well analyzed by the CEF model because the excited-state pseudotriplet is thermally occupied, and the ground state of the Ce(2) site can be regarded as a doublet. By contrast, the intensity at 1.0 K (blue circles) decreased compared with that at 15.3 K (red circles), and this decrease in intensity cannot be explained by the ground-state doublet. The pseudotriplet is not considered thermally occupied at 1.0 K. Therefore, in Eq. (2) we assume that one of the ground doublets shown in Fig. 2(f) is the ground state ( $\Delta_1 = 0$ ) and the other is the excited state ( $\Delta_2 \neq 0$ ). This is in agreement with the assumption that the Ce(2) sites share a ground-state pseudosinglet with two atoms, and accordingly, we changed the factor from 4 to 2 in Eq. (3). With these

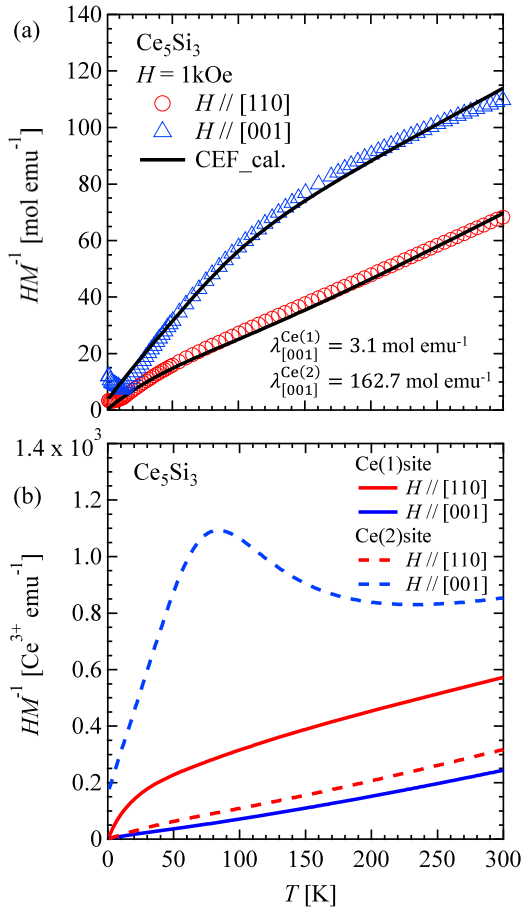


FIG. 4. (a) Temperature dependence of the reciprocal magnetic susceptibility of  $\text{Ce}_5\text{Si}_3$ . The red circles and blue triangles denote the measurement data for  $H // [110]$  and  $[001]$ , respectively, and the black solid lines were calculated using the CEF model. (b) Temperature dependence of the reciprocal magnetic susceptibility of the Ce(1) site (solid lines) and Ce(2) site (broken lines). The red and blue lines show the calculation results of  $H // [110]$  and  $H // [001]$ , respectively.

assumptions, the fitting result described the experimental results well [black broken line in Fig. 3(b)]; the parameters obtained based on this fitting are listed in Table I. At the aforementioned temperatures, the CEF parameters did not change considerably, and the CEF level schemes were almost the same. The largest change was evident in  $B_4^1$  at the Ce(1) site, where the increase indicates enhanced hybridization of  $|\pm 5/2\rangle$  and  $|\pm 3/2\rangle$  of  $\Gamma_7$ , probably due to changes in CEF effects in the ordered state. Our assumptions strongly support the splitting of the ground-state doublet due to spin-dimer formation.

Figure 4(a) shows the temperature dependence of the reciprocal magnetic susceptibility of  $\text{Ce}_5\text{Si}_3$ . The red circles and blue triangles show the measurements along the  $H // [110]$  and  $[001]$  directions, respectively, and the black solid lines show the reciprocal magnetic susceptibility calculated using the CEF parameters, which were obtained from the INS experiments at 15.3 K, and these behaviors explained the experimental data well. As the natural crystal growth planes of the single-crystal sample of  $\text{Ce}_5\text{Si}_3$  are (110) and (001),

magnetic susceptibility measurements were performed at  $H // [110]$  instead of  $H // [100]$ . When the atom responsible for magnetism occupied one site, the reciprocal magnetic susceptibility was described as  $\chi^{-1} = \chi_{\text{CEF}}^{-1} + \lambda$ , and the molecular field parameters  $\lambda^{\text{Ce}}$  were determined by fitting using Eq. (4) because the cerium atoms responsible for magnetism occupy two sites in this compound:

$$\chi = \frac{\chi_{\text{CEF}}^{\text{Ce}(1)}}{1 + \lambda^{\text{Ce}(1)} \chi_{\text{CEF}}^{\text{Ce}(1)}} + 4 \frac{\chi_{\text{CEF}}^{\text{Ce}(2)}}{1 + \lambda^{\text{Ce}(2)} \chi_{\text{CEF}}^{\text{Ce}(2)}}. \quad (4)$$

The fitting resulted in a molecular field of  $\lambda^{\text{Ce}(1)} = 3.1 \text{ mol emu}^{-1}$  and  $\lambda^{\text{Ce}(2)} = 162.7 \text{ mol emu}^{-1}$  along  $H // [001]$ . By contrast, the contribution of the molecular field was not considered along  $H // [110]$  because, as shown in Fig. 4(a), the behavior of magnetic susceptibility can be explained without the contribution of the molecular field. Figure 4(b) shows the temperature dependence of the reciprocal magnetic susceptibility of the Ce(1) (solid lines) and Ce(2) (broken lines) sites, and the red and blue lines show the calculation results for  $H // [110]$  and  $H // [001]$ , respectively. At the Ce(1) site, the reciprocal magnetic susceptibility in  $H // [110]$  was larger than that in  $H // [001]$ , and the easy axis caused by the CEF ground state was in the out-of-plane direction. This result explains the notable change in magnetic susceptibility at  $\chi_{[001]}$  compared with  $\chi_{[100]}$  at  $T_N \simeq 12 \text{ K}$ , where the magnetic moment of the Ce(1) site was magnetically ordered with an out-of-plane direction [24]. Although  $\lambda^{\text{Ce}(2)}$  is larger than  $\lambda^{\text{Ce}(1)}$ , as shown in Fig. 4(b), magnetic anisotropy at the Ce(2) site was unaffected, and the molecular field  $\lambda^{\text{Ce}(2)}$  estimated using the fitting function was effective. Furthermore, the Ce(2) site, in contrast to the Ce(1) site, exhibited an in-plane magnetic easy axis. Therefore, spin dimers are formed by magnetic moments oriented along the in-plane direction. The CEF parameters were obtained for the INS experiments at 1.0 K; the magnetic properties described above remained consistent with these parameters. The CEF levels have been reported in previous studies using magnetic susceptibility data [25,26]. The signs of the CEF parameters obtained at this study are consistent with the results of these previous studies. However, the energy levels obtained in this study are significantly different from those reported in these previous studies. The present study, which uses INS and magnetic susceptibility data, provides more accurate CEF levels of  $\text{Ce}_5\text{Si}_3$ .

## B. Spin-dimer excitation

To investigate the Schottky-type anomaly observed at around  $T_d = 2.5 \text{ K}$  in the specific heat measurement of  $\text{Ce}_5\text{Si}_3$ , INS measurements were performed at an incident energy of  $E_i = 3 \text{ meV}$ . Figure 5 shows the color-coded plots of INS intensities of (a)  $\text{Ce}_5\text{Si}_3$ , (b) nonmagnetic isostructural  $\text{La}_5\text{Si}_3$ , and (c) magnetic components of  $\text{Ce}_5\text{Si}_3$ . In  $\text{La}_5\text{Si}_3$ , no anomaly was observed, whereas in  $\text{Ce}_5\text{Si}_3$ , magnetic excitation was observed at around  $E = 0.6 \text{ meV}$ . This gap of approximately 0.6 meV agreed well with the size of the excited level ( $\Delta_d \sim 8 \text{ K} = 0.69 \text{ meV}$ ) calculated from the peak position of the Schottky-type anomaly observed in the specific heat measurements [12]. As the CEF excitations were determined as in Sec. III A, this excitation was not caused by the CEF effect. The excitation could be attributed to the magnetic

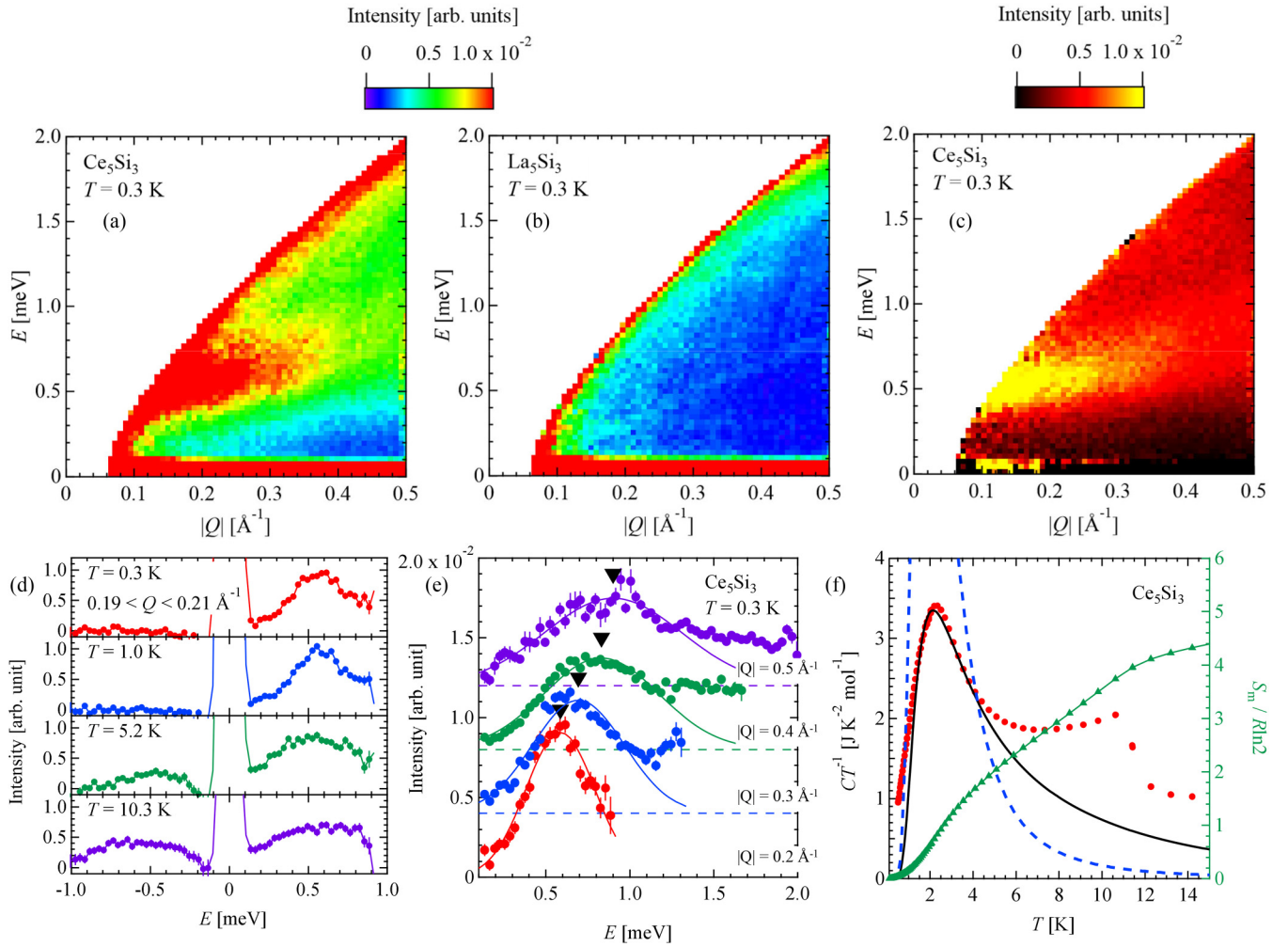


FIG. 5. Color-coded plots of INS intensity measured on HRC with  $E_i = 3$  meV for (a)  $\text{Ce}_5\text{Si}_3$  and (b)  $\text{La}_5\text{Si}_3$ , and (c) magnetic scattering of  $\text{Ce}_5\text{Si}_3$  at 0.3 K. (d) Temperature evolution of magnetic excitation at  $|Q| = 0.2 \text{ \AA}^{-1}$ . (e) Energy dependence of magnetic peaks at  $|Q|$ . The data were vertically shifted for clarity, and the dashed lines represent the origin of the vertical axis of the corresponding data. The solid lines represent the results of fitting each data with a Gaussian function, and the solid black triangles indicate the respective peak positions. The vertical bars in (d) and (e) represent statistical errors. (f) Temperature dependence of magnetic specific heat divided by temperature (red circles; left axis) and magnetic entropy (green triangles; right axis). The blue broken line and black solid line show the calculation curve when the excited pseudotriplet is assumed to be degenerate and not degenerate, respectively.

order of the Ce(1) site; however, the magnetic propagation vector for this compound was  $q = (001) = 0.465 \text{ \AA}^{-1}$  [29], which was inconsistent with the excitation. A  $(1\ 1\ 1)$  magnetic Bragg peak was observed in our INS experiment, and the absence of the  $(0\ 0\ 1)$  peak may be due to the orientation factor with the magnetic moment along the  $(0\ 0\ 1)$  direction. As the excitation appeared to rise from  $|Q| = 0 \text{ \AA}^{-1}$ , the possibility of spin-wave excitation due to ferromagnetism was considered; however, there are no previous reports of anomalies in specific heat or magnetic susceptibility associated with ferromagnetic transition or spontaneous magnetization [12,24,25]. In addition, the possibility of the ground-state splitting due to internal magnetic fields affected by magnetically ordered Ce(1) sites was considered; however, the expected excitation in this splitting must be flat like other CEF excitations. Therefore, this excitation was attributed to the splitting of the ground-state doublet of the  $\text{Ce}^{3+}$  ions with  $J = 5/2$  into

a ground-state pseudosinglet and excited-state pseudotriplet, which was associated with spin-dimer formation. The isolated dimer model exhibits a  $Q$ -dependent intensity with  $I(Q) \propto 1 - \sin QR / QR$  peaked at  $Q$  corresponding to the distance  $R$  between magnetic atoms forming the dimer [30]; however, the magnetic excitation observed herein did not follow this behavior. The same SSL material, i.e.,  $\text{SrCu}_2(\text{BO}_3)_2$ , did not exhibit the intensity that followed the isolated dimer model and indicated that the intensities of the singlet-to-triplet excitations peaked at the reciprocal lattice and superlattice points [31]. Thus, the magnetic excitations of  $\text{Ce}_5\text{Si}_3$  and  $\text{SrCu}_2(\text{BO}_3)_2$ , which cannot be explained by the isolated dimer model, may feature dimer excitations from the SSL model. This microscopic result suggests spin-dimer formation in the cerium compounds.

Figure 5(d) shows the temperature evolution of magnetic excitation with  $0.19 \leq |Q| \leq 0.21 \text{ \AA}^{-1}$  corrected using

the Bose factor. The red, blue, green, and purple symbols represent the measurement data at 0.3, 1.0, 5.2, and 10.3 K, respectively. At 0.3 and 1.0 K, where only the ground state was occupied, excitation from the ground state was observed at around  $E = 0.6$  meV. By contrast, at 5.2 and 10.3 K, the excited state at approximately 0.6 meV was thermally occupied with increasing temperature, so that excitation was observed even around  $E = -0.6$  meV, where the incident neutron gained energy. This result suggests that the spin dimers do not disappear even when the excited levels due to spin-dimer formation were thermally occupied. The persistence of this dimer state may be related to the splitting width of the excited-state pseudotriplet, as discussed below.

The energy dependence of magnetic peaks at  $|Q|$  is shown in Fig. 5(e). The red, blue, green, and purple symbols represent a one-dimensional cutout at  $|Q| = 0.2, 0.3, 0.4,$  and  $0.5 \text{ \AA}^{-1}$ , respectively, with a width of  $0.02 \text{ \AA}^{-1}$ . The solid lines represent the results of fitting each data with a Gaussian function, and the solid black triangles indicate the respective peak positions. To clearly observe the data, an equal offset has been added with respect to  $|Q| = 0.2 \text{ \AA}^{-1}$ . This figure shows that in  $\text{Ce}_5\text{Si}_3$ , the magnetic excitation associated with spin-dimer formation exhibits a peak shift and dispersion from  $E = 0.55$  meV at  $|Q| = 0.2 \text{ \AA}^{-1}$  to  $E = 0.9$  meV at  $|Q| = 0.5 \text{ \AA}^{-1}$ . Here, the in-plane Brillouin zone boundary in the reciprocal lattice is approximately  $0.5 \text{ \AA}^{-1}$ , indicating that in  $\text{Ce}_5\text{Si}_3$ , the dispersion width of magnetic excitation is approximately 0.35 meV. Theoretical calculations show that as  $\alpha$  increases, the width of the dispersion increases and the gap size decreases [6]. In the limit for the dimer phase  $\alpha = 0.677$ , the spin-gap and nearest-neighbor interaction are expressed as  $\Delta/J \approx 0.23$ , where the width of dispersion is  $0.09J$ . Applying the observed gap size of 0.55 meV to  $\Delta/J \approx 0.23$  gives  $J = 2.4$  meV and a dispersion width of 0.22 meV. Therefore  $\text{Ce}_5\text{Si}_3$  is potentially closer to the plaquette-singlet phase than  $\text{SrCu}_2(\text{BO}_3)_2$ , and the spin dimers formed in  $\text{Ce}_5\text{Si}_3$  could contribute to dispersion through the interactions between SSL layers and interactions with magnetically ordered Ce(1) sites, or both.

Figure 5(f) shows the temperature dependence of magnetic specific heat divided by temperature  $CT^{-1}$  (red circles; left axis) and magnetic entropy  $S_m/R \ln 2$  (green triangles; right axis). The blue broken line shows the calculated curve assuming that the excited-state pseudotriplet is degenerate due to spin-dimer formation. At low temperatures below 1 K, the behavior observed in the specific heat measurements that cannot be explained by the Schottky-type anomaly can be attributed to  $c-f$  hybridization. According to the magnetic entropy, the expected entropy is not released near the Schottky-type anomaly, and the behavior of the specific heat with a tail on the high-temperature side of the Schottky peak cannot be explained, suggesting the possible splitting of the excited-state pseudotriplet. The black solid line shows the fitting results assuming the splitting of the excited-state pseudotriplet;  $\Delta_{d1} = 6.47(2)$  K,  $\Delta_{d2} = 16.21(15)$  K, and  $\Delta_{d3} = 29.55(99)$  K. If this fitting result is correct, the intermediate level of the pseudotriplet should be observed at approximately 1.4 meV. The intensity remains on the high-energy side in Fig. 5(e). However, this intensity is not observed as a peak. The reason for this is that the intermediate level may have a wave function

that cannot be excited much from the ground state. Therefore, it is difficult to conclude that this intensity is an intermediate level in this study. In addition, this fitting was performed in the range below 4.5 K, where the effect on  $T_N$  is very weak, and whether the excited-state pseudotriplet is actually splitting or not needs to be directly observed in INS experiments using single-crystal samples.

The behavior in spin-dimer systems with large splitting widths of excited states has not been reported for  $\text{SrCu}_2(\text{BO}_3)_2$  (32.48, 34.8, and 37.12 K) [19,31] in the SSL model and for  $\text{YbAl}_3\text{C}_3$  (14.15, 16.47, and 18.79 K) [2] in the  $4f$ -electron system. Therefore, in  $\text{Ce}_5\text{Si}_3$  the excited-state pseudotriplet caused by the formation of spin dimer is suggested to be split via the interactions between SSL layers and interactions with magnetically ordered Ce(1) sites. To investigate the effects of such interactions, it is considered to grow isostructural materials in which the Ce(1) sites do not magnetically order, or to replace elements by nonmagnetic lanthanum. It is interesting to note the origin of the spin-dimer formation of  $4f^1$  cerium atoms where the direct interaction is very weak. In the future we aim to grow similar materials, analyze the splitting pseudotriplet excitations suggested in this study via INS, and investigate the change in dimer excitations in a magnetic field. We expect that theoretical calculations in such unusual states will be developed.

#### IV. CONCLUSION

We performed INS experiments using  $\text{Ce}_5\text{Si}_3$  and observed CEF excitations and dimer excitation. CEF excitations were observed at 17 and 63 meV at the Ce(1) site and at 27 and 39 meV at the Ce(2) site. The results of the CEF model calculations described well the behavior of magnetic susceptibility. The magnetic easy axis at the Ce(1) site appeared in the out-of-plane direction and was consistent with the behavior at  $T_N \sim 12$  K observed in the magnetic susceptibility. By contrast, at the Ce(2) site, the magnetic easy axis appeared in the in-plane direction, suggesting that in-plane-oriented magnetic moments form spin dimers. In the low-energy neutron experiments, magnetic excitation was caused by spin-dimer formation. The temperature evolution of magnetic excitation revealed that the spin dimers did not disappear even when the excited levels due to spin-dimer formation were thermally occupied. This excitation exhibited large dispersion that cannot be explained using the conventional SSL model [6], and the  $|Q|$ -dependent intensity cannot be explained using the isolated dimer model [30]. This behavior may be a feature of the dimers formed by SSL and may be characteristic of a  $4f$ -electron system. A detailed analysis of the specific heat data suggested the possible splitting of the excited-state pseudotriplet. These behaviors cannot be explained using the conventional SSL model, and interactions between the SSL layers and with the Ce(1) site should be considered as possible explanations.

#### ACKNOWLEDGMENTS

The neutron scattering experiments performed on HRC at J-PARC MLF, Japan, were approved by the Neutron

Scattering Program Advisory Committee of the Institute of Materials Structure Science, High Energy Accelerator Research Organization (No. 2020S01 and No. 2021S01). D.U.

thanks Dr. T. Momoi for a valuable discussion of the SSL model. This work was supported by JSPS KAKENHI Grants No. JP17K14342 and No. JP21K03449.

- 
- [1] A. Ochiai, T. Inukai, T. Matsumura, A. Oyamada, and K. Katoh, Spin gap state of  $S = 1/2$  Heisenberg antiferromagnet  $\text{YbAl}_3\text{C}_3$ , *J. Phys. Soc. Jpn.* **76**, 123703 (2007).
- [2] Y. Kato, M. Kosaka, H. Nowatari, Y. Saiga, A. Yamada, T. Kobiyama, S. Katano, K. Ohoyama, H. S. Suzuki, N. Aso, and K. Iwasa, Spin-singlet ground state in the two-dimensional frustrated triangular lattice:  $\text{YbAl}_3\text{C}_3$ , *J. Phys. Soc. Jpn.* **77**, 053701 (2008).
- [3] A. Dönni, G. Ehlers, H. Maletta, P. Fischer, H. Kitazawa, and M. Zolliker, Geometrically frustrated magnetic structures of the heavy-fermion compound  $\text{CePdAl}$  studied by powder neutron diffraction, *J. Phys.: Condens. Matter* **8**, 11213 (1996).
- [4] A. Oyamada, S. Maegawa, M. Nishiyama, H. Kitazawa, and Y. Isikawa, Ordering mechanism and spin fluctuations in a geometrically frustrated heavy-fermion antiferromagnet on the Kagome-like lattice  $\text{CePdAl}$ : A  $^{27}\text{Al}$  NMR study, *Phys. Rev. B* **77**, 064432 (2008).
- [5] M. J. Harris, S. T. Bramwell, D. F. McMorrow, T. Zeiske, and K. W. Godfrey, Geometrical frustration in the ferromagnetic pyrochlore  $\text{Ho}_2\text{Ti}_2\text{O}_7$ , *Phys. Rev. Lett.* **79**, 2554 (1997).
- [6] Z. Weihong, C. J. Hamer, and J. Oitmaa, Series expansions for a Heisenberg antiferromagnetic model for  $\text{SrCu}_2(\text{BO}_3)_2$ , *Phys. Rev. B* **60**, 6608 (1999).
- [7] J. S. Gardner, M. J. P. Gingras, and J. E. Greedan, Magnetic pyrochlore oxides, *Rev. Mod. Phys.* **82**, 53 (2010).
- [8] M. J. P. Gingras and P. A. McClarty, Quantum spin ice: A search for gapless quantum spin liquids in pyrochlore magnets, *Rep. Prog. Phys.* **77**, 056501 (2014).
- [9] R. Sibille, E. Lhotel, V. Pomjakushin, C. Baines, T. Fennell, and M. Kenzelmann, Candidate quantum spin liquid in the  $\text{Ce}^{3+}$  pyrochlore stannate  $\text{Ce}_2\text{Sn}_2\text{O}_7$ , *Phys. Rev. Lett.* **115**, 097202 (2015).
- [10] J. G. Rau and M. J. Gingras, Frustrated quantum rare-earth pyrochlores, *Annu. Rev. Condens. Matter Phys.* **10**, 357 (2019).
- [11] J. Knolle and R. Moessner, A field guide to spin liquids, *Annu. Rev. Condens. Matter Phys.* **10**, 451 (2019).
- [12] M. Kontani, M. Senda, M. Nakano, J. M. Lawrence, and K. Adachi, Magnetic properties of  $\text{Ce}_5\text{Si}_3$ , *J. Magn. Magn. Mater.* **70**, 378 (1987).
- [13] B. Sriram Shastry and B. Sutherland, Exact ground state of a quantum mechanical antiferromagnet, *Physica B+C* **108**, 1069 (1981).
- [14] A. Koga and N. Kawakami, Quantum phase transitions in the Shastry-Sutherland model for  $\text{SrCu}_2(\text{BO}_3)_2$ , *Phys. Rev. Lett.* **84**, 4461 (2000).
- [15] J. Y. Lee, Y.-Z. You, S. Sachdev, and A. Vishwanath, Signatures of a deconfined phase transition on the Shastry-Sutherland lattice: Applications to quantum critical  $\text{SrCu}_2(\text{BO}_3)_2$ , *Phys. Rev. X* **9**, 041037 (2019).
- [16] J. Yang, A. W. Sandvik, and L. Wang, Quantum criticality and spin liquid phase in the Shastry-Sutherland model, *Phys. Rev. B* **105**, L060409 (2022).
- [17] A. Koga, Ground-state phase diagram for the three-dimensional orthogonal-dimer system, *J. Phys. Soc. Jpn.* **69**, 3509 (2000).
- [18] R. W. Smith and D. A. Keszler, Synthesis, structure, and properties of the orthoborate  $\text{SrCu}_2(\text{BO}_3)_2$ , *J. Solid State Chem.* **93**, 430 (1991).
- [19] H. Kageyama, K. Onizuka, Y. Ueda, M. Nohara, H. Suzuki, and H. Takagi, Low-temperature specific heat study of  $\text{SrCu}_2(\text{BO}_3)_2$  with an exactly solvable ground state, *J. Exp. Theor. Phys.* **90**, 129 (2000).
- [20] H. Kageyama, M. Nishi, N. Aso, K. Onizuka, T. Yosihama, K. Nukui, K. Kodama, K. Kakurai, and Y. Ueda, Direct evidence for the localized single-triplet excitations and the dispersive multitriplet excitations in  $\text{SrCu}_2(\text{BO}_3)_2$ , *Phys. Rev. Lett.* **84**, 5876 (2000).
- [21] M. E. Zayed, C. Rüegg, J. Larrea J., A. M. Läuchli, C. Panagopoulos, S. S. Saxena, M. Ellerby, D. F. McMorrow, T. Strässle, S. Klotz, G. Hamel, R. A. Sadykov, V. Pomjakushin, M. Boehm, M. Jiménez-Ruiz, A. Schneidewind, E. Pomjakushina, M. Stingaciu, K. Conder, and H. M. Rønnow, 4-spin plaquette singlet state in the Shastry-Sutherland compound  $\text{SrCu}_2(\text{BO}_3)_2$ , *Nat. Phys.* **13**, 962 (2017).
- [22] Y. Cui, L. Liu, H. Lin, K.-H. Wu, W. Hong, X. Liu, C. Li, Z. Hu, N. Xi, S. Li, R. Yu, A. W. Sandvik, and W. Yu, Proximate deconfined quantum critical point in  $\text{SrCu}_2(\text{BO}_3)_2$ , *Science* **380**, 1179 (2023).
- [23] K. Momma and F. Izumi, *VESTA 3* for three-dimensional visualization of crystal, volumetric and morphology data, *J. Appl. Crystallogr.* **44**, 1272 (2011).
- [24] Y. Ushida, T. Nishioka, and M. Kontani, Possible realization of the coexistence of dimer and antiferromagnetism in  $\text{Ce}_5\text{Si}_3$ , *Physica B: Condens. Matter* **259-261**, 110 (1999).
- [25] Y. Ushida, T. Nishioka, M. Kontani, and N. K. Sato, Experimental study on metamagnetism in  $\text{Ce}_5\text{Si}_3$ , *J. Phys. Soc. Jpn.* **70**, 513 (2001).
- [26] T. Nishioka, R. Kobayashi, T. Yasunami, H. Kato, M. Matsumura, and K. Kodama, Magnetic properties of  $\text{Ce}_5\text{Si}_3$  single crystal under pressure, *J. Phys. Soc. Jpn.* **76**, 45 (2007).
- [27] S. Itoh, T. Yokoo, S. Satoh, S. ichiro Yano, D. Kawana, J. Suzuki, and T. J. Sato, High resolution chopper spectrometer (HRC) at J-PARC, *Nucl. Instrum. Methods Phys. Res., Sect. A* **631**, 90 (2011).
- [28] M. Hutchings, Point-charge calculations of energy levels of magnetic ions in crystalline electric fields, *Solid State Phys.* **16**, 227 (1964).
- [29] R. Kobayashi, private communication about the magnetic propagation vector.
- [30] A. Furrer and H. U. Güdel, Interference effects in neutron scattering from magnetic clusters, *Phys. Rev. Lett.* **39**, 657 (1977).
- [31] B. D. Gaulin, S. H. Lee, S. Haravifard, J. P. Castellan, A. J. Berlinsky, H. A. Dabkowska, Y. Qiu, and J. R. D. Copley, High-resolution study of spin excitations in the singlet ground state of  $\text{SrCu}_2(\text{BO}_3)_2$ , *Phys. Rev. Lett.* **93**, 267202 (2004).